

Signatures of Jet-Induced Shocks in the ISM

I. INTRODUCTION AND MOTIVATION

In Rodger Blanford’s words, “microquasars are AGN for the impatient [people].” These binary systems, in which a star accretes matter onto a roughly solar-mass black hole (BH), have much in common with AGN: both types of systems have accretion disks, coronae of energetic electrons, and strongly-collimated, relativistic jets. Unlike AGN, however, microquasars sit closer to our telescopes and evolve on conveniently shorter timescales.

How jets launch from accreting BH systems remains unknown. The current picture implicates both general relativity and the strong magnetic fields that are thought to exist near the BH event horizon. If this model is correct, jets will, in some fashion, retain the fingerprints of the magnetic fields that flung them out from near the BH. If we know what percent of the accreting system’s energy is funnelled into these jets, we can therefore begin to place limits on the strength and the configuration of the magnetic fields present near the event horizon [1].

To measure the amount of energy pumped into a microquasar’s jets, we turn to the class of techniques laid out in this course. In particular, we want to correlate the amount and type of damage these jets inflict on the ISM with characteristics of the jets themselves. Examining the size of the bruise these jets leave on the ISM, so to speak, tells us how much of a punch they pack.

Jet impacts heat and ionize the low-density ISM via strong shocks. Shocks also come into play in many other astronomical situations, including supernova remnants, Herbig-Haro objects, and protostar winds. In all of these, the heated and ionized shock-front emits characteristic types of radiation, which contain information about the pre-shocked ISM density and the shock-front’s speed and energy.

The overall goals of this paper are to:

1. Briefly derive strong-shock conditions
2. Identify which emission features characterize strong shocks, and why
3. Derive what ISM conditions are required to produce those emission features, and
4. Show how to use those identifying features to derive the power contained in the agent responsible for the shock.

The paper concludes with a discussion of how these techniques have been applied to Cygnus X-1 and LMC X-1, both well-known BH systems.

II. THEORY

A. Shocks: Energy Input

Shock waves arise whenever material moves supersonically through an ambient medium. The shock front moves faster than information travels between gas particles in the ambient medium, meaning the upstream gas receives no ‘warning’ of the impending shock. The shock itself heats and

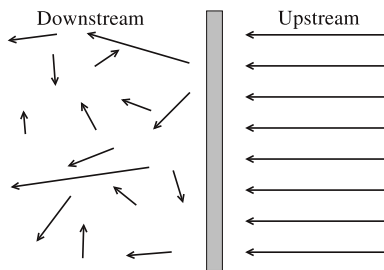


FIG. 1: Diagram of up- and down-stream gas velocities, relative to the shock front (grey box).

compresses the medium, leaving the gas changed in the wake of its passing. Later sections of this paper deal with precisely what changes that entails.

Two broad classes of shocks play important roles in astronomy. The simplest type, which we focus on in this paper, are strong, fast, so-called ‘jump shocks’ (a.k.a. J-shocks). The second type are slower, weaker, ‘continuous shocks’ (a.k.a. C-shocks), where magnetohydrodynamics plays an important role in shaping the shock’s structure. In short, the presence of a weak magnetic field allows neutral ions to broadcast information about the shock to the neutral upstream material, effectively broadening the shock [2]. This allows heating and cooling processes to equilibrate within the C-shock front [3]. Either increasing the ambient medium’s ionization fraction or ramping up the shock front’s velocity steepens a C-shock into a J-shock. In general, shocks moving faster than 40 km/s with respect to the ambient medium qualify as J-shocks [2]. Because jets excite swifter shocks than this [4], we hereafter confine our attention to J-shocks.

In J-shocks, the mean free path between particles in the ambient medium is longer than the width of the shock [3]. This means that density, velocity and pressure are, effectively, discontinuous across the shock front. By applying mass, momentum, and energy flux conservation across the shock front, we can derive the Rankine-Hugoniot jump conditions.

The problem becomes more tractable if we work in the frame moving with the shock. As illustrated in Figure 1, gas with well-ordered velocity moves into the shock from upstream, passes through the shock, and exits the shock downstream with higher entropy and disordered velocities. In the following analysis, which follows the standard derivation laid out in many texts [2, 3, 5], the subscripts u and d denote upstream and downstream quantities, respectively.

Conservation of mass flux across the shock front requires

$$\rho_u v_u = \rho_d v_d \quad (1)$$

Momentum conservation similarly requires

$$\rho_u v_u^2 + P_u = \rho_d v_d^2 + P_d \quad (2)$$

Finally, energy flux conservation tells us that the energy difference between the upstream and downstream gas is equal to the work done by the shock per unit area:

$$E_d - E_u = P_u v_u - P_d v_d \quad (3)$$

In the above, we define the energy flux as

$$E = \rho v \left(\frac{1}{2} v^2 + \frac{u}{\rho} \right) \quad (4)$$

The first term in the parenthesis represents the kinetic energy of the gas, while the second term represents the gas's internal energy. The internal energy, U , includes internal degrees of freedom, such as rotation and vibration, as well as the binding energy, of all chemical species in the gas. For an ideal gas, we can simply say

$$U = \frac{P}{\gamma - 1} \quad (5)$$

where γ represents the ratio of the specific heats of the gas. The ISM is not a monatomic gas. Within the shock front, however, the gas particles only suffer elastic collisions. Within the shock front, therefore, we can treat ISM as a monatomic gas [2], with

$$\gamma = \frac{5}{3}. \quad (6)$$

Equations 1, 2, 3, 4 and 5 can be combined and rearranged to yield

$$\frac{P_d}{P_u} = \frac{(\gamma - 1)\rho_u - (\gamma + 1)\rho_d}{(\gamma - 1)\rho_d - (\gamma + 1)\rho_u} \quad (7)$$

and

$$\frac{\rho_d}{\rho_u} = \frac{(\gamma - 1)P_d + (\gamma + 1)P_u}{(\gamma - 1)P_d + (\gamma + 1)P_u} \quad (8)$$

These two relations can be further simplified to

$$\frac{P_d}{P_u} = \frac{2\gamma}{\gamma + 1}M^2 - \frac{\gamma - 1}{\gamma + 1} \quad (9)$$

and

$$\frac{\rho_u}{\rho_d} = \frac{\gamma - 1}{\gamma + 1} + \frac{2}{\gamma + 1} \frac{1}{M^2} \quad (10)$$

where we define the Mach number as the ratio of the shock speed (measured relative to the upstream gas) to the (upstream) sound speed:

$$M = \frac{v_{s,u}}{C_{s,u}} \quad (11)$$

Recall that sound speed is defined [3] as

$$C_s = \left(\frac{dP}{d\rho} \right)^{1/2} = \left(\frac{\gamma P}{\rho} \right)^{1/2} \quad (12)$$

In the ISM, $C_s \approx 10$ km/s. Since the J-shocks we plan to study travel much faster than 40 km/s, we can safely say that $M \gg 1$. This, along with 6, lets us rewrite equations 9 and 10 to obtain the Rankine-Hugoniot shock conditions:

$$\frac{\rho_d}{\rho_u} = \frac{\gamma + 1}{\gamma - 1} = 4 \quad (13)$$

and

$$P_d = \frac{2}{\gamma + 1} \rho_u v_u^2 = \frac{3}{4} \rho_u v_u^2 \quad (14)$$

Equations 13 and 14 tell us two things:

1. The shock can increase the downstream gas pressure by an arbitrary amount, but
2. The shock can only enhance the downstream gas density by up to a factor of four.

The first condition, along with the ideal gas law, tells us that a shock can also increase the downstream gas temperature by an arbitrary amount. This lets us begin to discriminate shocked gas from photoionized gas. As we learned early in this course, heating and cooling processes within HII regions are in equilibrium, leading to characteristic gas temperatures around 10^4 K [3]. In shock-excited ISM, however, the temperature is given by [6]

$$T = 3.18 \times 10^5 \frac{(\text{shock velocity})^2}{10^4 \times \text{particles per H nucleus}} \text{ K} \quad (15)$$

Obviously, shock-excited gas easily reaches temperatures above 10^5 K. Provided the shock does not move through very high-density ISM, we can use [OIII] line ratios to take the excited region's temperature.

Because the gas cooling timescale is significantly longer than the length of the shock front's visit, no energy radiates from the shock front itself [3], meaning that the shock front is isothermal. Only after the front has passed can the gas start to shed the energy deposited by the shock. This is where the second result from above proves important, as the gas's cooling timescale depends inversely on density. Post shock gas with a column density less than

$$N_{crit} \approx 2 \times 10^{17} \left(\frac{v_u}{100 \text{ km/s}} \right)^{4.2} \text{ cm}^{-2} \quad (16)$$

will not radiate efficiently [2]. Because a shock can only increase the ISM density by a finite amount, it must move through sufficiently dense (upstream) material if we hope to detect its afterglow.

B. Spectra: Energy Output

The light shocked material emits depends on what ionization species are present. Collisional ionization rates greatly exceed photoionization rates in the region immediately behind the shock [7] There, particles suffer many collisions, leading the collisional ionization and electron recapture processes into equilibrium. Casting this in an equation, which we quote from Osterbrook [3], we see:

$$n(X^{+i})n_e q_{ion}(X^{+i}, T) = n(X^{+i+1})n_e \alpha_G(X^{+i}, T) \text{ cm}^{-3}\text{s}^{-1} \quad (17)$$

The collisional ionization rate coefficient, q_{ion} , depends only on the electron temperature and the ion's collisional ionization cross section. It does not, however, depend on the electron density. This means that the post-shock temperature sets which ionization species get produced [3]. For typical post-shock temperatures in the neighborhood of 10^5 K, this completely dissociates and ionizes all hydrogen, and creates a rich population of low-ionization state metals. Collisions between electrons

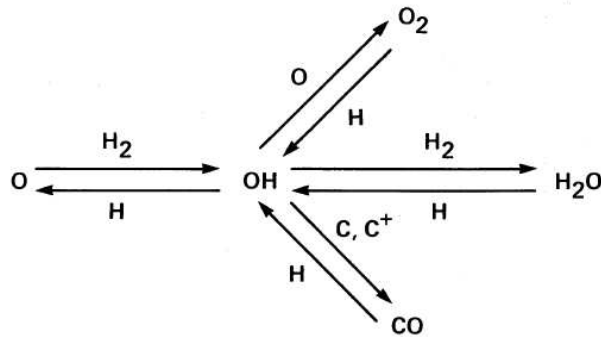


FIG. 2.—Fast neutral reactions with moderate activation energies or endothermicities dominate the oxygen chemistry in warm $T \gtrsim 300$ K postshock gas.

FIG. 2: Figure from [6], showing the neutral H chemistry driving molecular dissociation behind the shock.

and atoms usher atomic electrons into and out of so-called metastable states. As a result, we expect to see strong forbidden-line transitions from low-ionization metal species in shock-ionized gas. In contrast, we expect to see mostly highly ionized species in HII regions. Table I, adapted from Osterbrock [3], bears out the comparison.

Ion	Wavelength (Angstroms)	Orion (photoionized)	Cas A (shock-heated)
[OII]	3727	1.47	1.28
[OIII]	4363	0.0139	0.22
H β	4861	1.00	1.00
[OIII]	4959	1.00	1.12
[OIII]	5007	3.02	3.38
[OI]	5577	0.00058	0.07
[OI]	6300	0.00012	0.31
[NII]	6583	0.596	2.98
[SII]	6717	0.0314	1.15

TABLE I: Table adapted from [3], showing the observed emission-line relative intensities in shock-heated and photoionized environments.

As Figure 2 shows, the hydrogen dissociated by the shock efficiently dismantles CO, O₂ and H₂O. We therefore expect not to see rotational and vibrational molecular emission until H₂ recombines far downstream.

Figure 3 outlines the temperature structure and cooling mechanisms at work behind the shock. We can think of the shocked gas undergoing two phase transitions, much as water does during its transitions from steam to liquid, and from liquid to ice. In this case, however, ionized atoms, neutral atoms, and molecules take the place of steam, liquid, and ice, respectively.

The dissociated, ionized gas is initially transparent to Ly α recombination photons. These, along with bremsstrahlung radiation, cool the gas to $\approx 10^4$ K. By that point, enough neutral hydrogen has re-formed to make the gas opaque to UV and optical photons. The temperature plateaus at 10^4 K, as photoionization and recombination come into (near) equilibrium— just as they do in HII regions.

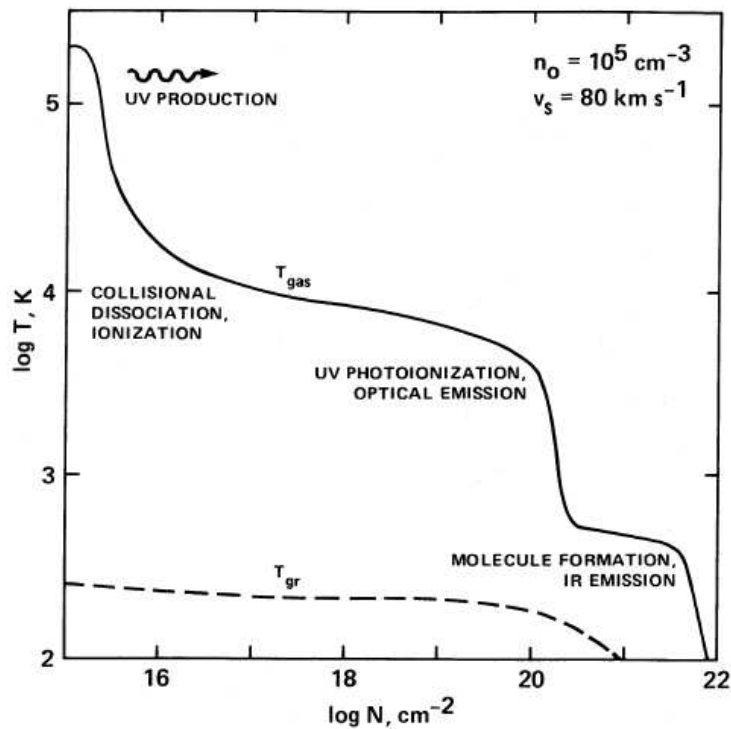


FIG. 1.—The postshock temperature structure of a fast molecular shock ($n_0 = 10^5 \text{ cm}^{-3}$, $v_{s,7} = 0.8$ shown here). Three regions are delineated: (1) the hot, $T \sim 10^5 \text{ K}$, immediate postshock region, where gas is collisionally dissociated and ionized and UV photons are produced which affect both the pre-shock and postshock gas; (2) the “recombination plateau,” where the Lyman continuum photons are absorbed, maintaining $T \sim 10^4 \text{ K}$; and (3) the recombining and molecule-forming gas downstream, where chemical energy of H_2 formation can maintain a lower temperature plateau (*see text*). The column densities of the first two regions are nearly independent of n_0 . Note that the grains are weakly coupled to the gas, so that $T_{\text{gr}} \ll T_{\text{gas}}$.

FIG. 3: Figure from [6], showing the post-shock temperature profile.

Unlike in an HII region, however, there is no steady supply of photons. Once enough UV/optical photons escape the system, the temperature drops again. At temperatures of $\approx 7 \times 10^3 \text{ K}$, H_2 (along with CO , O_2 and H_2O) recombination provides a second reservoir of latent heat, and create a second, lower temperature plateau. After the second plateau, molecules, which recombined in high vibrational and rotational states, give off IR photons as they cool to lower states [8]. In this final region, then, we expect to observe strong vibrational and rotational lines.

Putting all of these characteristics together lets us separate shock-ionized ISM from photoionized ISM. In particular, higher values of [OI] $\lambda 6300, 6364$, [OII] $\lambda 3727$, [OIII] $\lambda 4959, 5007$, and [SII] $\lambda 6717, 6731$ flux with respect to $\text{H}\alpha$ are the spectroscopic fingerprints of radiative shocks [9].

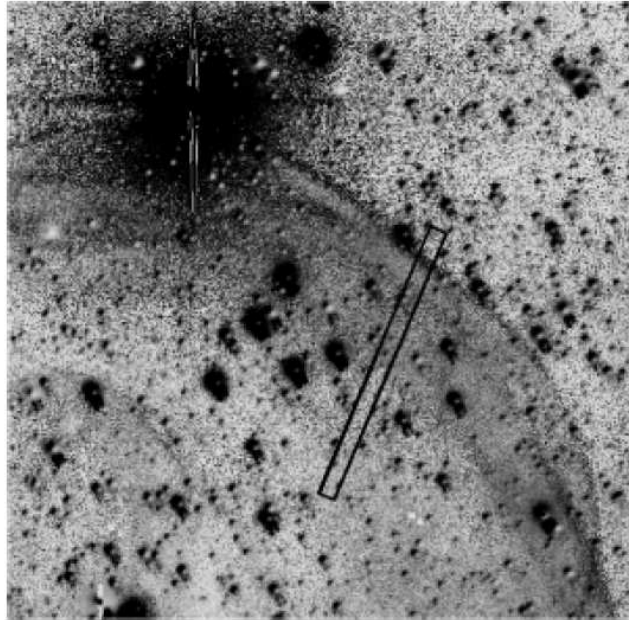


Figure 5. A blow-up of part of Fig. 2c: $[\text{O III}] / \text{H}\alpha$ image of the Cyg X-1 ring nebula. We interpret the thin outer shell with a high $[\text{O III}] / \text{H}\alpha$ flux ratio as possibly originating in the ionised atoms close to the front of the bow shock. North is up, east to the left. The emission line fluxes and $[\text{O III}] / \text{H}\alpha$ ratio along the slice indicated in the image are shown in Fig. 6.

FIG. 4: Figure from [10], showing an identifying feature of shock-excited ISM.

III. APPLICATIONS

Now that we have a set of tools for identifying shocked gas, we look at how they can help us to locate microquasar tracks in the ISM. Two groups have recently used these techniques to gather evidence of intermittent and/or ‘dark’ jets in Cygnus X-1 and LMC X-1.

The first, led by Gallo, Fender, Kaiser and Russell, observed a typical bow-shock structure near Cyg X-1 [4]. Follow-up observations found strong $[\text{OIII}]/\text{H}\alpha$ flux ratios shortly behind the shock, as shown in Figure 4[10].

As we saw above, a narrow region of bright $[\text{OIII}]$ emission is a signature of shocked ISM. This, together with the bow-shock shape of the emitting region, provides strong evidence of jet-shocked ISM near Cyg X-1. Russell et al also used the $[\text{OIII}]/\text{H}\alpha$ ratio to find the speed of the shock. The brightness of the radiative bow-shock also constrains how much power the shock has deposited into the ISM. Surprisingly, this suggests the jet, when active, may carry off 60-100% of the black hole’s total accretion power [4].

LMC X-1 sits inside the nebula N159. If this BH xray binary also produces jets, it therefore stands a good chance of producing observable jet-shock signatures. In fact, Cooke et. al. [11] recently observed $[\text{OI}]$, $[\text{NII}]$, $[\text{SII}]$, He I, and $[\text{ArIII}]$ lines near LMC X-1. However, it remains unclear how much of this emission is due to shock ionization, and how much arises from x-ray photoionization.

Because [OIII] emission characterizes both x-ray photoionization and shock ionization, the authors turn to [ArIII]/HeI and [SII]/H α line ratios to find a shock speed of $v_s \approx 90$ km/s. This lets them estimate the jet's power, which should be 60-100% of LMC X-1's total observed accretion power. However, it is found to be ten times larger than LMC X-1's current accretion power. This suggests that, unlike the 'dark' jet observed in Cyg X-1, the LMC X-1's jets are transient, and are currently off.

IV. SUMMARY

We have examined the hydrodynamics and chemistry of strong shocks. From that physical foundation, we derived the unique signatures strong shocks leave on the IM. The unique temperature and ionization pattern (UV and optical line emission, followed by IR emission) downstream of the shock, along with the enhanced ratios of forbidden line flux from low ionization species metals relative to H α , let us distinguish shock-excited gas from photoionized gas. Finally, we looked at how those tools have recently been used to ferret out information about possible jets in the microquasar sources of Cygnus X-1 and LMC X-1.

-
- [1] A. K. J. Frank and D. Raine, *Accretion Power in Astrophysics* (Cambridge University Press, 2002), 3rd ed.
 - [2] A. Tielens, *The Physics and Chemistry of the Interstellar Medium* (Cambridge University Press, 2005).
 - [3] D. Osterbrock and G. Ferland, *Astrophysics of Gaseous Nebulae and Active Galactic Nuclei* (University Science Books, 2006), chap. 6, pp. 157–175, 2nd ed.
 - [4] C. K. e. a. E. Gallo, R. Fender, *Nature* **436**, 819 (2005), URL doi:10.1038/nature03879.
 - [5] F. Shu, *Astronomy 202 course reader*, Berkeley Copy Mat (1990), chapters 15 and 19.
 - [6] D. Hollenbach and C. McKee, *ApJ* p. 306 (1989).
 - [7] Y. Fadeyev and D. Gillet, *A& A* pp. 423–435 (2004).
 - [8] C. Hollenbach and McKee, *ESA SP* pp. 245–258 (1988).
 - [9] B. Fesen and Kirshner, *ApJ* pp. 29–48 (1985).
 - [10] G. Russell, Fender and Kaiser, *MNRAS* pp. 1341–1349 (2007).
 - [11] R. S. R. Cooke, Z. Kuncic and J. Bland-Hawthorn, *ApJ* **667**, L163 (2007), URL <http://arxiv.org/abs/0708.2314>.